

Titanium with aligned, elongated pores for orthopedic tissue engineering applications

Erik D. Spoerke,^{1*} Naomi G.D. Murray,¹ Huanlong Li,² L. Catherine Brinson,^{1,2} David C. Dunand,¹ Samuel I. Stupp^{1,3,4}

¹Department of Materials Science and Engineering, Northwestern University, Evanston, Illinois 60208

²Department of Mechanical Engineering, Northwestern University, Evanston, Illinois 60208

³Department of Chemistry, Northwestern University, Evanston, Illinois 60208

⁴Department of Materials Science and Engineering, Department of Chemistry, Feinberg School of Medicine, Northwestern University, Evanston, Illinois 60208

Received 6 February 2006; revised 4 January 2007; accepted 30 January 2007

Published online 6 July 2007 in Wiley InterScience (www.interscience.wiley.com). DOI: 10.1002/jbm.a.31317

Abstract: Porous titanium with elongated and aligned pores, mimicking the anisotropic structure of bone, was created by solid-state expansion of argon trapped in elongated pores between titanium wires. Both elastic moduli and yield strengths are larger in the longitudinal direction ($E = 51$ GPa, $\sigma_y = 338$ MPa) than in the transverse direction ($E = 41$ GPa, $\sigma_y = 267$ MPa). Finite-element analysis of simplified anisotropic structures provides insight into the local micromechanical behavior of these porous materials, evaluating elastic modulus, resistance to plastic deformation, and localized stress concentrations which may be experienced under biological loading. Preliminary *in vitro* cell culture studies further demonstrate the influence of the

elongated porous microstructure on osteoblast colonization behavior. These studies suggest that as an optimized material, titanium with aligned, elongated pores is promising for applications in orthopedic tissue engineering, as it combines high strength, toughness, and biocompatibility of titanium with the reduced stiffness and open porosity suitable for mechanical integration with bone tissue produced by aligned pores. © 2007 Wiley Periodicals, Inc. *J Biomed Mater Res* 84A: 402–412, 2007

Key words: titanium foam; anisotropy; bone; orthopedic tissue engineering; mechanical properties; finite-element; osteoblasts

INTRODUCTION

Titanium and its alloys are used in orthopedic and dental applications wherein their excellent strength-to-weight ratio, toughness, corrosion resistance, and surface oxide biocompatibility have proven widely successful.^{1–4} Still, titanium lacks the ability to form a strong interface with surrounding tissue and its relatively high stiffness can lead to stress shielding of surrounding bone and subsequent implant loosening. One approach to resolving the problem of interfacial

strength has been to use porous surfaces, relying on tissue ingrowth into the shallow porous surface layer to create a strong mechanical interface with surrounding tissue. Another approach uses titanium foam, which exhibits porosity not only near the implant surface but throughout its volume. In addition, fully porous titanium offers reduced stiffness, which addresses the problem of stress shielding. Titanium with varying levels of porosities can be produced by a range of sintering methods,⁵ including partial sintering of powders^{6,7} or coiled wires,⁸ or by sintering of powders around a temporary space-holding phase,^{9,10} but the resulting structures are relatively weak, because of the small size of the necks connecting the individual powder particles.

An alternative foaming method for titanium alloys was developed by Kearns et al.^{11,12} Micrometer-size bubbles of pressurized argon are entrapped within a titanium matrix during densification of titanium powders by hot isostatic pressing. Upon subsequent exposure to elevated temperatures at ambient pressure or vacuum, these bubbles expand by creep of the surrounding titanium matrix, resulting in the formation of a titanium foam with up to 50% porosity. Compared with porous titanium produced by powder sintering,

*Present address: Electronic and Nanostructured Materials, Sandia National Laboratories, Albuquerque, NM 87123, USA.

†Present address: Stryker Howmedica Osteonics, 300 Commerce Court, Mahwah, NJ 07430, USA.

Correspondence to: S. I. Stupp; e-mail: s-stupp@northwestern.edu

Contract grant sponsor: The National Science Foundation; contract grant numbers: DMR-0108342 and DMR-0505772

Contract grant sponsor: The National Institutes of Health; contract grant number: R01 DE015920-01A1

these foams exhibit higher strength because of the more rounded pore shape and full density of struts.¹³ In an adaptation of this process, Dunand and coworkers^{13–17} have described the use of transformation superplasticity to create highly porous titanium foam. In this process, a densified titanium billet, containing pressurized argon bubbles, is thermally cycled through the HCP-BCC phase transformation. The pressurized argon trapped in the billet serves to bias the lattice mismatch strains created during the thermal cycling, allowing for superplastic expansion of the gas-filled pores.

Recent studies of porous titanium for orthopedic applications have focused largely on creating equiaxed pores.^{18,19} Bone, however, has elongated, aligned pores leading to structural and mechanical anisotropy,^{20–24} an adaptation that provides greater strength and stiffness along directions of applied physiological stresses. Taking cues from this biological model, porous titanium implants with highly aligned, elongated pores could be useful as orthopedic implant materials.

Titanium foams with anisotropic porosity have rarely been previously described in the literature. Kearns et al.^{11,12} originally demonstrated a type of anisotropic pore structures by rolling or extruding a densified, argon-containing powder preform of HIPed powder prior to isothermal foaming. No micrographs of elongated pores were provided, but anisotropic expansion during foaming was indicative of nonequiaxed pores. Davis et al.¹⁴ described a method of applying a directional load during the foaming by transformation superplasticity of a titanium-powder-based foam. Creep deformation resulted in the elongation of the forming pores to an average aspect ratio of about 2 (and maximum value of 5), aligned in the direction of the applied load. In both of these alternative methods, additional processing was required, either before or during foaming, to create the porous anisotropy.

In this paper, we describe a new method for the direct solid-state synthesis of titanium containing aligned, highly elongated pores, by replacing the titanium powders used in the existing argon expansion method with thin titanium wires. We present microstructural and mechanical characterization of the resulting anisotropic porous titanium, finite-element model predictions to elucidate its micromechanical behavior as a potential implant material, and initial *in vitro* cell response to the elongated porous microstructure.

MATERIALS AND METHODS

Processing

Wire of commercial-purity titanium (CP-Ti, Grade II) from Alfa Aesar (Ward Hill, MA) with 250 μm diameter was cut into pieces of 55 mm length and packed lengthwise in a steel canister with an inner diameter of 19 mm to about 47% den-

sity. The wire-packed canister was evacuated and back-filled with 0.7 MPa argon. The wires were densified by hot isostatic pressing at 890°C with 100 MPa for 120 min by Bodycote, IMT, Inc. (Andover, MA). Specimens with $5 \times 5 \times 10 \text{ mm}^3$ dimension were cut by electrodischarge machining from the densified billet. Foaming of these specimens took place by expansion of argon-filled micropores under transformation superplasticity conditions, previously demonstrated with spherical titanium powders.^{13–16} In this process, radiant heating was used to thermally cycle the specimen between 830 and 980°C with a 4-min cycle period under a flowing argon atmosphere (1 atm). This temperature range spans the allotropic temperature range of CP-Ti (nominally at 882°C but expected to be higher and wider due to oxygen content).²⁵ For comparison of the foaming behavior, control samples were foamed isothermally at 903 or 1250°C under 1–5 mTorr residual argon atmosphere. The lower temperature of 903°C is the effective temperature of the above-mentioned thermal cycle. This temperature is defined as the temperature at which the isothermal creep rate is the same as the time-averaged creep rate during thermal cycling in the absence of transformation superplasticity,^{26,27} found by using lattice activation energies given by Frost and Ashby²⁸ for α -Ti and β -Ti. By comparing the thermal cycling foaming kinetics with those at the effective temperature, the effect of superplasticity on foaming is directly revealed. The high temperature of 1250°C was selected as a temperature sufficiently high to insure complete exhaustion of the internal pore pressure during foaming to produce relatively high, open porosity.

Frequent interruptions by excursions to room temperature occurred during foaming to determine specimen porosity. Archimedes density measurements were carried out on all specimens in distilled water. A thin layer of vacuum grease was used to seal the surface of each specimen in order to prevent infiltration of water into the open porosity, yielding a direct measurement of the total porosity (sum of open and closed porosity). Density measurements were also performed using helium pycnometry with an Accupyc 1330 (Micromeritics, Norcross, GA) on unsealed specimens, allowing for measurement of the closed porosity.

An as-densified sample and a specimen foamed under thermal cycling conditions were each sectioned parallel and perpendicular to the wire length using a low-speed diamond saw, mounted in acrylic resin, and polished to 0.05- μm alumina. Porous specimens were vacuum-infiltrated with acrylic resin at regular intervals during polishing, filling open porosity to retain the original pore shape during polishing.

Mechanical testing and modeling

Foamed specimens were cut by electro-discharge machining into parallel pipeds $3 \times 3 \times 6 \text{ mm}^3$ in dimension, with equal numbers of samples ($n = 4$) cut parallel and perpendicular to the direction of wire orientation. These samples were deformed under axial compression along their long dimension at a rate of 0.5 mm/min. Sample strain was recorded with a laser extensometer. Each sample was cycled twice through an elastic loading and unloading from 0–1500 N before increasing the load to induce plastic deformation. Elastic modulus was measured as the linear slope on a stress-strain plot of the second unloading; the estimated error was

TABLE I
Young's Modulus (E) Poisson's Ratio (ν), and Yield Stress (σ_{yield}) Used for Finite Element Analysis

	E (GPa)	ν	σ_{yield} (MPa)
Titanium	110	0.33	275
Bone	20	0.30	120

1 GPa. Yield stress was determined as 0.2% deviation from linearity in a plot of stress *versus* strain of the final loading.

Finite-element (FE) modeling was used to derive theoretical predictions of the microscale and macroscale mechanical behaviors of these porous structures. Unit cell models were created for spherical pores (aspect ratio 1), short elliptical pores (aspect ratio 3), and long elliptical pores (aspect ratio 6); see Figure 6. The porosity of the models was 12%, matched to the experimentally obtained porosity described in the results below. Pores were evaluated both empty or filled with bone to simulate the effects of bone growth into the pores. The material properties used for the simulations are displayed in Table I. The elastic modulus, yield strength, and strain hardening behavior for titanium were determined from a stress-strain curve for CP-40 titanium,²⁹ and values for dense cortical bone were obtained from the literature.^{20,22,30} Because of the lack of reliable data for plasticity hardening curves for bone, an elastic-plastic approximation was used. A commercial FE software package (ABAQUS Standard 6.3-1) was used to create three-dimensional (3D) meshes, representative of titanium matrices containing pores of the three different aspect ratios. Standard 20-node quadratic brick elements were defined for the entire geometry. Mesh convergence was verified based on overall and local stress values.

For the 3D models, a negative displacement was applied on top or right surface of the 3D models to simulate the uniaxial compressive loading in either the longitudinal (long axis, y -axis) or transversal (short axis, x -axis) direction to study the responses. The boundary conditions are defined as follows: the center of the pore was fixed and the surface perpendicular to the loading direction was also fixed in the direction normal to the surface. The four faces parallel to loading direction were constrained to remain planar and normal to one of the coordinate axes throughout the computations. Therefore, the boundary conditions for the unit cell models can be considered as periodic. Simulations were conducted to determine the sample moduli, stress concentration factors, and onset of local plasticity by incremental displacement for the models.

In this study, simple periodic boundary conditions were used to simulate an array of perfectly aligned, smooth ellipsoidal pores. Since the unit cells are 3D models, they avoid the overestimation of stress and strain localization observed in 2D porous models.³¹ Modest deviations in the pore shapes from perfectly smooth ellipsoids have been shown to be relatively unimportant for overall mechanical properties.³² However, other works on porous Ti modeling^{33,34} have shown that spatial randomization of the porous microstructure has a significant influence on properties which will not be captured by the single pore unit cell models here. Because of the difficulty in obtaining a representative volume element for the degree of microstructural irregularity demonstrated by the experimental samples (Fig. 3),³³ random microstructures

were not modeled. Thus, it is expected that the FE results will overpredict the magnitudes of the modulus, while local stress concentrations will be underpredicted, compared to the experimental values. Nevertheless the trends for the impact of pore shape and the effect of bone ingrowth will be captured and are useful to understand the effects of these parameters on mechanical performance of Ti with elongated aligned pores.

Evaluating osteoblast colonization

In vitro cell response to the anisotropic porous titanium was probed using primary rat long bone osteoblasts. Osteoblasts were cultured in a T-75 culture flask in MEM- α , supplemented with 10% fetal bovine serum, 1% penicillin streptomycin, and 50 $\mu\text{g}/\text{mL}$ ascorbic acid. At $\sim 80\%$ confluence, cells were removed from the T-flask by treatment with 0.25% trypsin, 1 mM ethylenediaminetetraacetic acid (EDTA). Trypsinization was stopped by addition of culture medium and cells were collected by centrifugation.

Samples with 12% porosity produced after 15-h thermal cycling were cut with an abrasive alumina wheel into $\sim 3 \times 3 \times 1 \text{ mm}^3$ in dimension. This cutting process produced smearing artifacts, which covered some pores. These pores were gently reopened by etching in 0.25% HF, 2.5% HNO₃ for 45 min and repassivated in 40% HNO₃ for 40 min. Rinsed thoroughly with water, samples were autoclaved for 45 min at 121°C. Samples were then placed in a 24-well tissue culture polystyrene plate. Two passages after harvest, 10,000 cells were placed in each well containing a porous sample. Samples were allowed to culture for 5 days, changing culture medium at day 3. At day 5, samples were removed and fixed for 1 h in 2.5% glutaraldehyde in 0.1M sodium cacodylate buffer. Specimens were rinsed thoroughly in sodium cacodylate buffer and then postfixed in 1% osmium tetroxide for 1 h. Following thorough rinsing with water, samples were dehydrated in graded ethanol (50, 70, 80, 90, 95, 100%) for 10 min each. Dehydrated samples were then critical point dried by CO₂ exchange and sputter-coated with 3 nm of Au-Pd for viewing by scanning electron microscopy. Microscopy was performed at 20 kV and 20 μA using a Hitachi S-4500 scanning electron microscope.

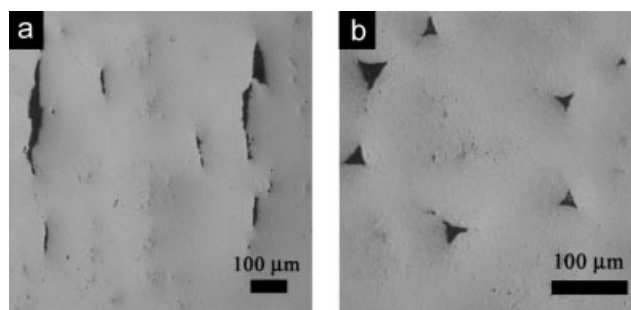


Figure 1. Longitudinal (a) and transverse (b) optical micrographs of hot isostatically pressed wire billet prior to foaming, showing large, elongated pores in the space between the wires.

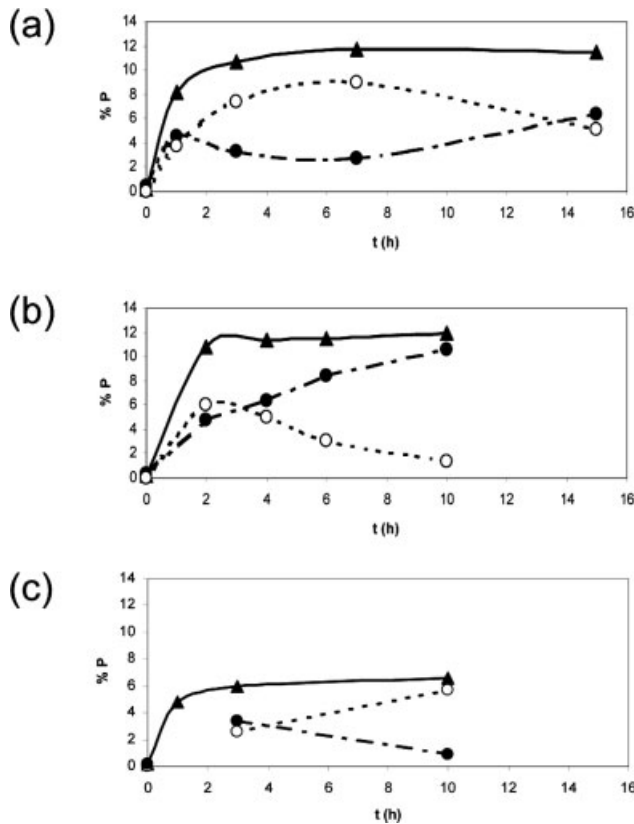


Figure 2. Plots of porosity *versus* time for foams created by thermal-cycling (830–980°C) (a); high-temperature isothermal treatment at 1250°C (b); and low-temperature isothermal treatment at 903°C (c), corresponding to the effective temperature of the thermal cycles. Plots show the temporal evolution of total porosity (▲), open porosity (○), and closed porosity (●).

RESULTS

Processing and structure

The porosity of the as-densified billet was determined to be 0.27%. Figure 1(a,b) shows the as-densified pore structure parallel and perpendicular to the length of the original wires, respectively. It is apparent that the argon-pressurized pores in the densified material retained the elongated shape of the gap between the wires in the original preforms.

Figure 2 shows the total porosity as a function of time for specimens foamed under thermal cycling or isothermal conditions at either 903 or 1250°C. Foaming under superplastic thermal cycling conditions resulted in a higher total porosity than did foaming under isothermal creep conditions at the effective temperature of the thermal cycle (903°C). Isothermal foaming at 1250°C, however, led to similar foaming kinetics and total porosity to thermal cycling (~12% total porosity in both cases). Figure 2 also shows the open and closed porosity of specimens foamed under thermal cycling

and isothermal conditions, along with the total porosity. In all three cases, as the total porosity increased, the amount of open porosity also increased, as pores coalesced with each other and channels opened to the specimen surface. After ~2 h of isothermal foaming at 1250°C and 7 h of thermal cycling, however, the measured open porosity decreased, though the thermally cycled specimen produced the highest final percentage of open pores. Because the thermally cycled specimen produced both the highest open and highest total porosity, characteristics of principal interest for orthopedic applications, the remaining characterization described in this paper will focus on thermally cycled specimens.

The pore structure after thermal cycling is shown in Figure 3(a,b). Parallel to the length of the wires [Fig. 3(a)], large (in the range of 1 mm), elongated pores were generally aligned along the original wire length. The apparent aspect ratio of the pores varied widely from ~2 to 25, and the pores seemed uniformly distributed within the volume. In the perpendicular direction [Fig. 3(b)], the pore cross sections were roughly equiaxed and also uniformly distributed. Figure 3(a,b) both show evidence of pore coalescence. Furthermore, a high number of much smaller equiaxed pores (below 50 μm in size) are visible in both Figure 3(a,b), localized

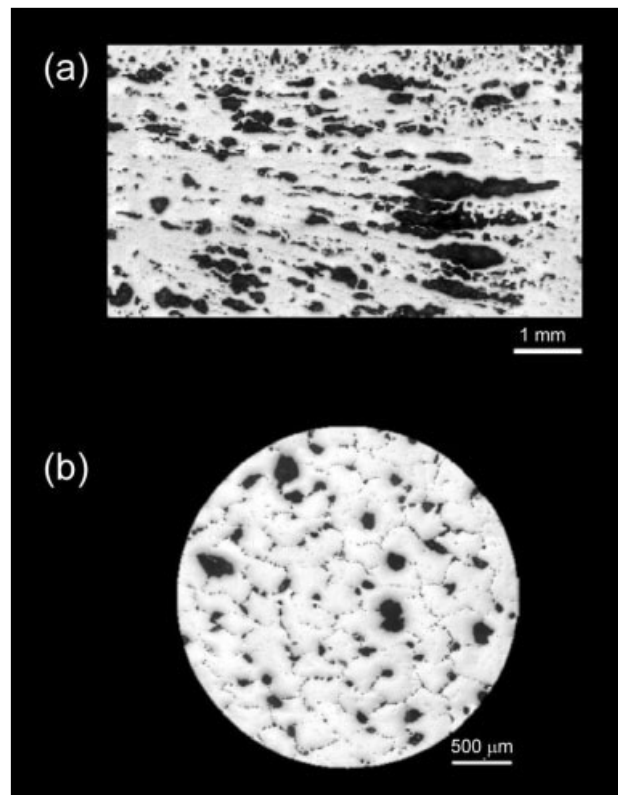


Figure 3. Longitudinal (a) and transverse (b) optical micrographs of 12% porous anisotropic titanium foam created by thermal cycling. Both large, elongated, aligned pores and small, equiaxed pores are visible.

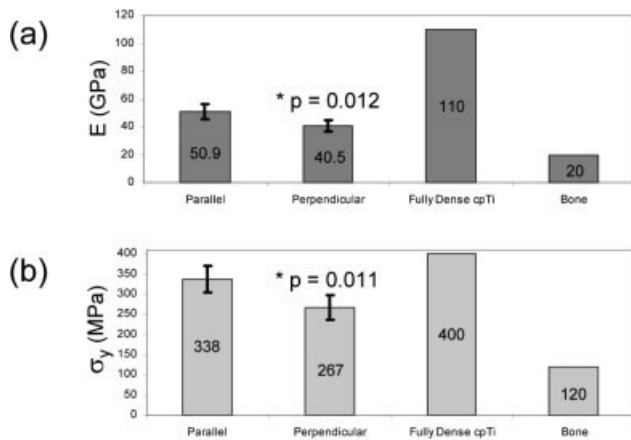


Figure 4. Elastic modulus (a) and yield stress (b) measured on 12% porous anisotropic titanium foam created by thermal cycling. Compressive measurements were performed at room temperature with loading direction either parallel or perpendicular to the long axis of the pores. The p values are for a 95% confidence interval.

at the prior surface of the wires. These pores were probably created by expansion of very small argon filled bubbles at the wire interfaces, not visible in Figure 1(a,b).

Mechanical testing and modeling

Compression testing of the thermally cycled material with 12% porosity [shown in Figs. 3(a,b)] demonstrated anisotropy of both elastic modulus (E) and compressive yield strength (σ_y), as shown in Figure 4. At 95% confidence both characteristics are found to be statistically higher in the longitudinal (parallel) direction ($E = 51$ GPa, $\sigma_y = 338$ MPa) than in the transverse (perpendicular) direction ($E = 41$ GPa, $\sigma_y = 267$ MPa). The magnitude of the elastic modulus is also noteworthy, as the porosity reduced the specimen stiffness under both longitudinal and transverse loading by more than half as compared to dense titanium, such that the values of modulus were closer to natural bone ($E = 20$ GPa) than fully dense titanium ($E = 110$ GPa).

The FE modeling examined the local micromechanical response of the matrix around the pores. Figure 5 shows the quantitative results of these models, while Figure 6 provides a visual representation of these data in the corresponding von Mises stress maps. First, the FE models predicted anisotropy of the elastic modulus in models containing elongated pores. The moduli were found to be higher for longitudinal loadings than for transverse loadings [Fig. 5(a)], a result consistent with the empirical measurements described earlier. Furthermore, this anisotropy, as described by the calculated anisotropy factors in Table II, was related to the aspect ratio of the pores, with the most elongated pore model demonstrating the greatest anisotropy. The elas-

tic moduli under longitudinal loading of the elliptical pore models were markedly greater than in the spherical model, while transverse loading moduli were only slightly reduced. Compared with the experimental data, the predicted moduli are higher and the anisotropy factor smaller because the random pore distribution and very high aspect ratio pores are not included in the models.

Understanding that the FE models are overestimating mechanical properties, the models can be used to better understand the trends of important mechanical response not easily obtainable by experimentation: local stress concentrations, onset of local plasticity, and effect of bone infiltration. In Figure 6, 3D maps depict the distribution of von Mises stress in a quadrant of

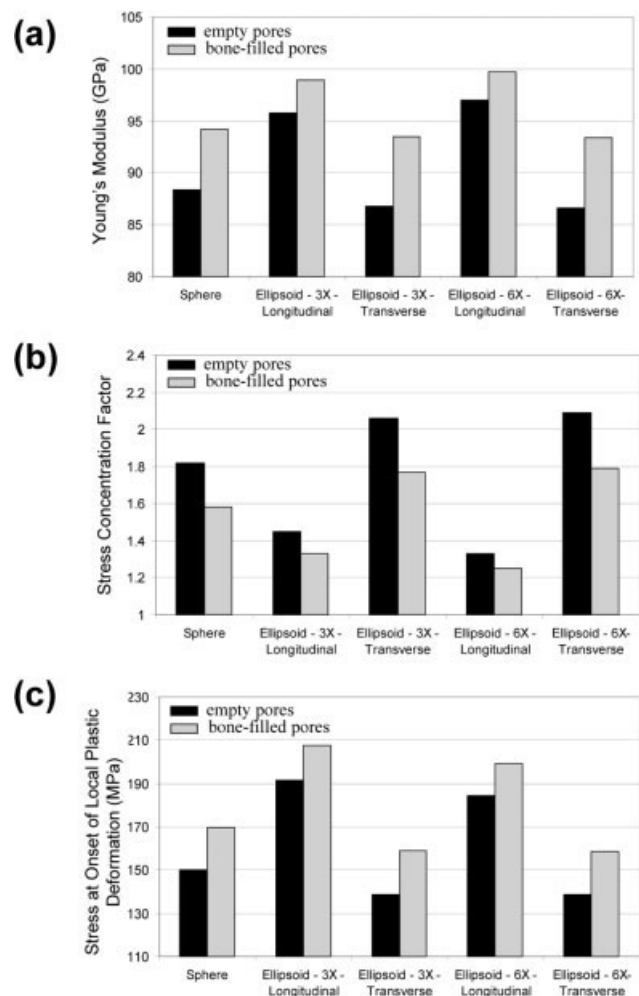


Figure 5. Micromechanical properties around a single pore of 12% porous anisotropic titanium determined by finite-element analyses: Young's moduli (a), stress concentration factors (b), and onset of local plastic deformation (c). Plot compares values under longitudinal (y) and transverse (x) loading as determined for a spherical pore (aspect ratio 1), a slightly elliptical pore (aspect ratio 3), and a more elliptical pore (aspect ratio 6). Plot also shows comparison of calculated values for empty pores and pores filled with simulated bone tissue.

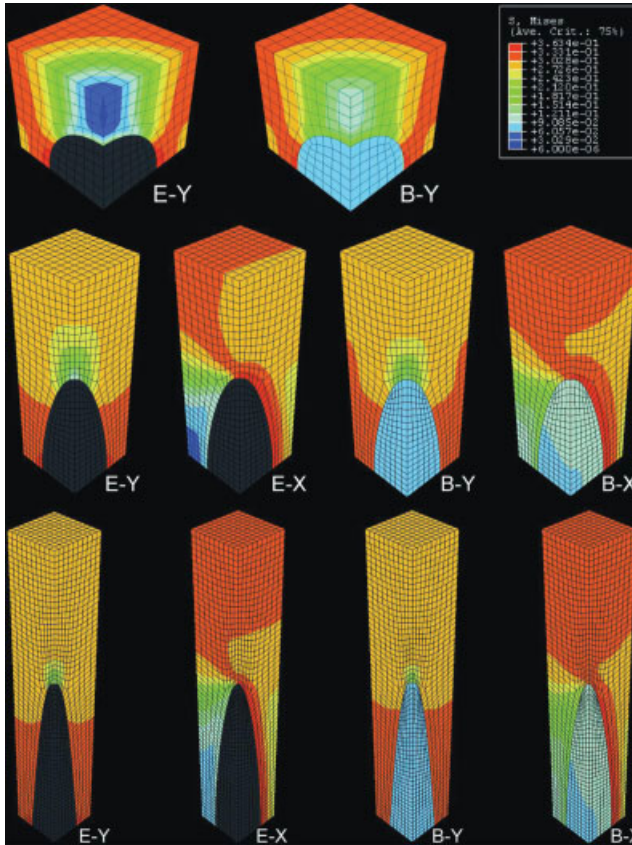


Figure 6. Maps of von Mises equivalent stresses in 12% porous titanium containing pores of aspect ratios 1, 3, and 6 (top, middle, and bottom, respectively) Maps are labeled according to their contents (E, empty; B, bone-filled) and the direction of loading with respect to the long axis of the pores (Y, longitudinally; X, transversely).

each model under longitudinal and transverse loadings. All longitudinally loaded samples showed the highest stress values midway down the periphery of the pore, while the lowest stresses were found to be localized near the top of the pores. Although the transverse loading for the spherical model was identical (rotated 90 deg) to the longitudinal loading, the elliptical pore models showed the highest stresses localized along the right periphery of the pore, with the lowest stresses found just off of the left side of the pore. Figure 5(b) provides a more quantitative evaluation of stress distribution in these specimens, displaying a stress concentration factor for each pore type under both longitudinal and transverse loading. Stress concentration factors were determined as

$$[\sigma] = \frac{\sigma_{\max}}{\sigma_{\text{average}}}$$

These stress concentrations were found to be significantly higher under transverse (x) loadings than longitudinal (y) loadings for both elliptical models.

Moreover, the aspect ratio of each pore was found to influence the distribution of stresses in each model. Higher aspect ratios yielded higher stress concentrations in the transverse loadings, but lower stress concentrations for the longitudinal loadings. This effective variation in the anisotropy of the stress concentrations is reflected in the calculated anisotropy factors of Table II.

In addition to the Young’s modulus and the stress concentration, the onset of local plastic deformation was examined by FE modeling. Figure 5(c) plots the stress at the onset of local plastic deformation in each foam model. For loads applied longitudinally, the onset of local plastic deformation was delayed for both types of elliptical pores when compared with spherical pores. In addition, the values in Table II show that for foams with elongated pores, the delay in plastic deformation was greater for longitudinally applied loads than the corresponding acceleration for transversely applied loads. These results also show that the change from spherical to ellipsoidal pores had moderate influence on the mechanical properties of porous titanium while the difference between pores of 3:1 and 6:1 aspect ratio had less influence.

The FE models also revealed the effects of filling the pores with bone. As evident in Figures 5 and 6, for each model, the presence of bone inside the pore increased the Young’s modulus, redistributed and reduced stress concentrations, and delayed the onset of local plastic deformation. These effects were most pronounced in the transverse loading cases and the spherical pore model. The calculated anisotropy factors, shown in Table II, were also affected by the ingrowth of bone such that the effective anisotropy seen in the two elliptical models was diminished for each material property. Note that the anisotropy factors for the stress concentration factors were increased towards unity, which corresponds to a reduction in anisotropy. The comparative trends between the bone-filled models of each pore shape were consistent with the trends observed for the models containing no bone.

Osteoblast colonization

In vitro cell culture studies revealed the influence of this anisotropic foam structure on primary rat osteoblastic cells. Figure 7 contrasts the morphologies of cells cultured on a flat titanium surface [Fig. 7(a)] and cells cultured on the anisotropically porous foam [Figs. 7(b,c)]. The cell in Figure 7(a), cultured on a flat surface, has adopted a characteristic fibroblastic shape with a strong leading edge (bottom right), a flattened cell body, and a distinctive tail (top left). In contrast, the morphology of cells that encountered the porous channels of the foam was dramatically affected by the foam microstructure. Cells significantly elongated themselves preferentially along the contours of the pores,

TABLE II
Measured Values and Calculated Anisotropy Factors (Property Under Longitudinal Loading Divided by Property Under Transverse Loading) Determined by Finite Element Calculation on Foams With 12% Pores of Three Different Aspect Ratios

	Young's Modulus		Stress Concentration Factor		Stress at Onset of Local Plastic Deformation	
	Value (Gpa)	Anisotropy Factor	Value	Anisotropy Factor	Value (Mpa)	Anisotropy Factor
<i>Without bone</i>						
Sphere (aspect ratio 1)	88.4	1	1.82	1	150.3	1
Ellipsoid (aspect ratio 3)						
L	95.8	1.10	1.45	0.70	191.6	1.37
T	86.8		2.06		138.9	
Ellipsoid (aspect ratio 6)						
L	97.0	1.12	1.33	0.64	184.3	1.33
T	86.6		2.09		138.6	
<i>With bone</i>						
Sphere (aspect ratio 1)	94.2	1	1.58	1	169.6	1
Ellipsoid (aspect ratio 3)						
L	98.9	1.06	1.33	0.75	207.7	1.31
T	93.5		1.77		159.0	
Ellipsoid (aspect ratio 6)						
L	99.7	1.07	1.25	0.70	199.2	1.25
T	93.4		1.79		158.8	

Anisotropy factors farther from unity (either greater than 1 or less than 1) indicated more anisotropic behavior. L represents longitudinal (*y*-axis) and *T* represents transverse (*x*-axis) loading.

even climbing inside porous channels. These behaviors are depicted in Figure 7(b,c).

DISCUSSION

Processing and structure

It is apparent from Figure 2(a–c) that superplastic, thermal-cycling pore expansion produces higher foaming rates and higher terminal porosity than isothermal pore expansion at the effective temperature of the thermal cycle, a result consistent with previous reports on isotropic foams made using spherical powders.^{13–17} Still, the isothermal pore expansion at the high temperature of 1250°C showed similar foaming rates and terminal porosities when compared with pore expansion by thermal cycling at much lower temperatures (830–980°C), indicating that slower deformation rates under creep conditions can be compensated by higher temperatures. In all three cases studied—*isothermal pore expansion at 903 and 1250°C, and thermal cycling—the porosity began to open to the specimen surface early in the pore expansion process. This process led to the escape of the pressurized argon gas and cessation of the growth of the pores open to the surface. As seen in Figure 2, however, for the thermal cycling and high-temperature isothermal cases, open porosity starts to decrease when total porosity reaches a maximum value. This effect may be due to sintering of depressurized pores connected to the surface by small necks, dis-*

connecting individual or connected pores from the sample surface. The hypothesis that sintering (which is diffusion controlled and thus sensitive to temperature) is responsible for this effect is supported by the observation that, after 10 h of foaming, the decrease in open porosity is small or nonexistent for the two specimens foamed at lower temperature (903 and 830–980°C) and large for the specimen foamed at high temperature (1250°C).

From a tissue engineering standpoint, porous titanium would ideally have relatively high total porosity to reduce implant stiffness, while retaining maximum open porosity for tissue ingrowth. The superplastically foamed titanium produced the highest values of both total and open porosity. As Figure 2 reveals, superplastic pore expansion would optimally have been terminated after about 7 h, when these porosity values had achieved their maximum, and before sintering began to close open pores. By comparison, foams made at the thermally effective temperature (903°C) maintained high open porosity, but the total porosity was about twice as low. On the other hand, the high-temperature isothermal treatment (1250°C) produced a total porosity similar to that achieved under superplastic thermal cycling, but the maximum open porosity (6% after 2 h of foaming) was only about two-thirds that of the superplastic sample (9% after 7 h). Furthermore, extreme grain growth and contamination of titanium by residual gases, which both degrade its mechanical properties, are much more likely to occur at this very high temperature. While the pore size visible in metallographic section [Fig. 3a,b)] is sufficient for bone

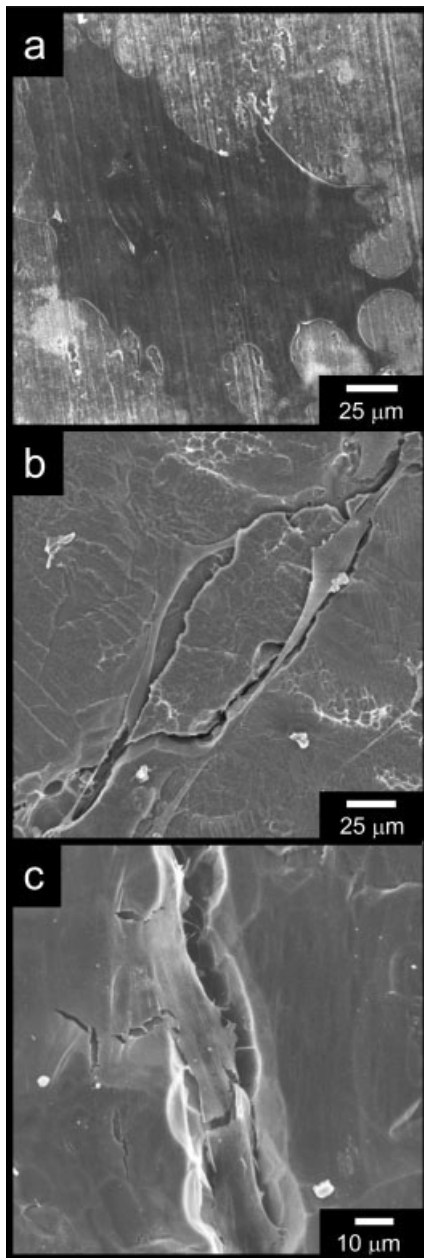


Figure 7. Scanning electron micrographs of primary rat osteoblasts growing on a flat titanium surface (a) and along elongated pores (b and c) of titanium with 12% anisotropic pores. The cell on the flat titanium surface has adopted a typically flat, spread morphology, while cells on pores are seen extending along and climbing down into pores.

ingrowth, it is not known whether constrictions exist at the points where pores merged, which could prevent ingrowth. Opening of such constrictions may however be possible by subsequent acid dissolution.

Unlike previously reported methods for making anisotropic foams,^{11,12,14} the elongated morphology of the pores in the present materials is directly related to the elongated shape of the titanium precursor (wires) used initially. Pores formed during consolidation of these wires are highly elongated [Fig. 1(a)], and it is apparent

that the subsequent expansion of these elongated pores does not lead to spheroidization (low apparent aspect ratios exhibited by some of the pores in Figure 3(a) may be due to the lack of alignment with the metallographic plane). The creation of elongated pores through the use of titanium wire as a precursor material demonstrates how pore morphology may be modified. In previous reports, it was shown that spherical precursor materials (powders) produced roughly spherical pores,^{12,14} which could, however, sometimes link into tortuous cavities with high overall aspect ratios but no preferred orientation. By comparison, the use of elongated starting materials (wires) produced elongated pores in the final product with much smoother walls and straighter shapes and with excellent orientation. Future work with other alternative materials shapes may yield other pore morphologies of technological interest. In addition, because the variation in pore morphology described here depends largely on the precursor materials and not on complex intermediate processing stages, mixed morphologies may be created. For example, wires could be used together with powders to create foams with mixed porous character, or foams with gradients in pore shape and/or volume fractions. Such an approach may be particularly appropriate in trying to mimic the complex architecture of bone.

While the present method has shown strong potential for the synthesis of anisotropic foams, our initial results show a relatively low porosity (12%) by traditional foam standards. This relatively low porosity is believed to be at least partly due to nonoptimal hot-isostatic pressing conditions, a factor which could be improved. Individual wires are still visible both before and after foaming (see Figs. 1 and 3), and the as-densified microstructure in Figure 1(a) reveals relatively large voids between sintered fibers. This condition likely caused premature foaming cessation as the limited bonding area between neighboring wires may have allowed growing pores to easily open to the surface of the specimen. As shown in Figure 2, at least half of the porosity is open to the specimen surface after about 2 h of foaming under thermal cycling conditions. These conditions are likely responsible for the relatively low porosity of the present materials and strongly suggest that the porosity could be increased with optimized densification. Another factor that may have contributed to the moderately low porosity of the present specimens is the relatively large wire diameter (250 μm) as compared to the specimen size (5 \times 5 \times 10 mm^3). Recent reports have shown that superplastically foamed titanium created using large diameter powders (400 μm) was significantly less porous than foams produced using powders with diameters under 200 μm .¹⁷ Although comparisons between these experiments and the present work ignore any geometric considerations, the powder findings suggest that the use of smaller

diameter wires and larger billets may further increase the final foam porosity. Nonetheless, the present experiments have demonstrated that this solid-state approach is an effective method for making porous titanium with significant structural and mechanical anisotropy. Additionally, even at this relatively low porosity, this porous titanium has demonstrated potential for application in orthopedic tissue engineering, as discussed in greater detail below.

Mechanical testing and modeling

The aligned pore morphology and resulting mechanical behavior created a material more closely resembling natural bone than a fully dense, isotropic titanium implant. Elongated porosity has the potential to address issues of implant reduction in weight and stiffness while minimizing strength reduction in the direction of loading. The aforementioned mechanical tests and FE analyses describe a system with reduced stiffness, a characteristic that would, in principle, help relieve problems with stress shielding by more effectively sharing applied stresses with surrounding bony tissue. In fact, the mechanical testing showed that the elastic modulus (under both longitudinal and transverse loading) was closer in magnitude to bone than to solid Ti. Though still lower than the values for fully dense Ti, the FE analysis projected moduli higher than the experimental results, a difference due to the fact that the FE analysis examined only a perfectly periodic array of smooth, ellipsoidal pores, while the mechanical testing results represent the influence from a random distribution of pores of different sizes, aspect ratios, and severe shape irregularities. The stiffness anisotropy of porous titanium also parallels the anisotropy of natural bone's stiffness and may help to promote stress sharing with surrounding bone in a more natural way. In addition to the changes in modulus, these porous materials demonstrated greater strength experimentally and were predicted to have greater resistance to local plastic deformation in the longitudinal direction than in the transverse direction. This mechanical anisotropy, directed by the engineered pore structure, represents an important similarity to the mechanical behavior of natural bone. Such similarity suggests that this type of porous material may be well adapted to provide strong mechanical support of the directional loads applied in biological systems. By adapting porous titanium to the types of loads they are likely to experience in a body, implant performance and durability may be enhanced. It is also interesting to note that for the specific periodic geometries chosen, the greatest predicted resistance to local plastic deformation was found in the ellipsoidal pores with aspect ratio 3. This effect suggests that not only is it advantageous to create elongated pores, but that there may be an optimal pore

geometry for an implant. Such a system would balance the advantages of the pores' anisotropy with the best resistance to deformation.

The FE modeling also described how the infiltration of bony tissue into the porous structure might affect the mechanical behavior of the implant. According to the models, significant infiltration of these pores with bony tissue would modestly increase the overall stiffness of the implant structures, as one would expect, while remaining below the values of fully dense Ti. More important, though, the models suggest that this bony tissue would serve to reduce and redistribute stress concentrations found in the titanium matrix, which would be expected to help extend implant lifetimes. Moreover, that the bone is serving to redistribute stress within the implant requires that the bone share a fraction of the applied stress. The resulting stress-induced stimulation of this bony tissue would be likely to promote bone growth³⁵⁻³⁷ and may help create a more stable and secure bone-implant interface.

Osteoblast colonization

The preliminary *in vitro* results illustrated an interesting interaction between osteoblasts and the porous surfaces. Cells readily attached and spread on the specimen biocompatible TiO₂ surface, even crawling into the elongated pores. Such healthy cell attachment and ingrowth would likely lead to the formation of a strong implant-tissue interface. In addition, these results are consistent with previous reports demonstrating directed cell growth using grooved surface features.^{38,39} The directional influence on cell growth observed in the present case suggests that this structurally and mechanically anisotropic material may be capable of influencing early stages of new tissue growth, serving as a directional template to newly forming bone. Certainly, cellular organization and behavior in tissues such as bone are directed by the anisotropic nature of its matrix. By directing the organization of biological materials with this anisotropic, nonbiological porous titanium template, it may be possible to better promote natural cellular organization and activity associated with the artificial implant. Further *in vivo* studies with anisotropic porous titanium may help to explore this issue.

CONCLUSIONS

We have demonstrated the creation of aligned, highly elongated pores in titanium by a two-step process consisting of (i) entrapping argon into elongated pores during high-temperature densification of bundled titanium wires and (ii) expansion of these pores by creep or superplastic deformation of the surrounding

metal. This anisotropic microstructure yielded anisotropy of both measured and computationally predicted strength and stiffness. Characteristics, such as higher elastic modulus, yield strength, and higher resistance to deformation when loaded longitudinally than when loaded transversely, mimic behavior of natural bone. In addition, the overall decrease in the modulus when compared with dense titanium is expected to reduce the effects of stress shielding associated with fully dense implants, while the high longitudinal strength would help support directional loads to be experienced by the implant. The influence of the elongated porous microstructure on osteoblastic colonization of these structures suggests that not only is mechanical integration of tissue with these materials possible, but the pores may be able to direct the form and function of newly forming tissues. These studies suggest that in an optimized form, titanium with an anisotropic pore structure shows excellent promise for orthopedic tissue engineering.

The authors thank Dr. Robert Satcher of the Orthopaedic Surgery Department at the Northwestern University Feinberg School of Medicine for providing the rat long bone osteoblasts. They also thank Mr. Scott Oppenheimer for his assistance with the high-temperature isothermal foaming, and Prof. Hui Shen, now at Ohio Northern University, for guidance and assistance with the finite element modeling.

References

- Urban R, Jacobs J, Sumner D, Peters C, Voss F, Galante J. The bone-implant interface of femoral stems with non-circumferential porous coating—A study of specimens retrieved at autopsy. *J Bone Jt Surg—Am Vol*, 1996;78A:1068–1081.
- Laing PG. Tissue reaction in rabbit muscle exposed to metallic implants. *J Biomed Mater Res* 1967;1:135–149.
- Hayashi K, Uenoyama K, Matsuguchi N, Sugioka Y. Quantitative analysis of *in vivo* tissue responses to titanium-oxide and hydroxyapatite-coated titanium alloy. *J Biomed Mater Res* 1991;25:515–523.
- Albrektsson T, Branemark PI, Hansson HA, Kasemo B, Larsson K, Lundstrom I, McQueen DH, Skalak R. The interface zone of inorganic implants *in vivo*: Titanium implants in bone. *Annals Biomed Eng* 1983;11:1–27.
- Dunand DC. Processing of titanium foams. *Adv Eng Mater* 2004;6:369–376.
- Asaoka K, Kuwayama N, Okuno O, Miura I. Mechanical properties and biomechanical compatibility of porous titanium for dental implants. *J Biomed Mater Res* 1985;19:699–713.
- Oh IH, Nomura N, Masahashi N, Hanada S. Mechanical properties of porous titanium compacts prepared by powder sintering. *Scripta Mater* 2003;49:1197–1202.
- Murray GAW, Semple JC. Transfer of tensile loads from a prosthesis to bone using porous titanium. *J Bone Jt Surg—Br Vol* 1981;63:138–141.
- Bram M, Stiller C, Buchkremer HP, Stover D, Baur H. High-porosity titanium, stainless steel, and superalloy parts. *Adv Eng Mater* 2000;2:196–199.
- Wen CE, Mabuchi M, Yamada Y, Shimojima K, Chino Y, Asahina T. Processing of biocompatible porous Ti and Mg. *Scripta Mater* 2001;45:1147–1153.
- Kearns M, Blenkinsop P, Barber A, Farthing T. Manufacture of a novel porous metal. *Met Mater* 1987;3:85.
- Kearns MW, Blenkinsop PA, Barber AC, Farthing TW. Manufacture of a novel porous metal. *Int J Powder Metall* 1988;24:59–64.
- Murray NGD, Dunand DC. Microstructure evolution during solid-state foaming of titanium. *Compos Sci Technol* 2003;63:2311–2316.
- Davis N, Teisen J, Schuh C, Dunand D. Solid-state foaming of titanium by superplastic expansion of argon-filled pores. *J Mater Res* 2001;16:1508–1519.
- Murray NGD, Dunand DC. Effect of thermal history on the superplastic expansion of argon-filled pores in titanium. II. Modeling of kinetics. *Acta Mater* 2004;52:2279–2291.
- Murray N, Dunand D. Effect of thermal history on the superplastic expansion of argon-filled pores in titanium. I. Kinetics and microstructure. *Acta Mater* 2004;52:2269–2278.
- Murray NGD, Dunand DC. Effect of initial preform porosity on solid-state foaming of titanium. *J Mater Res* 2006;21:1175–1188.
- Spoerke E, Murray N, Li H, Brinson L, Dunand D, Stupp S. Organoapatite-titanium foam: A bioactive composite for orthopedic tissue engineering. *Acta Biomater* 2005;1:523–533.
- Wen C, Yamada Y, Shimojima K, Chino Y, Hosokawa H, Mabuchi M. Novel titanium foam for bone tissue engineering. *J Mater Res* 2002;17:2633–2639.
- Weiner S, Wagner HD. The material bone: Structure-mechanical function relations. *Annu Rev Mater Sci* 1998;28:271–298.
- Bonfield W, Grynblas M. Anisotropy of the Young's modulus of bone. *Nature* 1977;270:453–454.
- Katz JL, Yoon HS. The structure and anisotropic mechanical properties of bone. *IEEE Trans Biomed Eng* 1984;31:878–884.
- Fan Z, Swadener JG, Rho JY, Roy ME, Pharr GM. Anisotropic properties of human tibial cortical bone as measured by nanoindentation. *J Orthop Res* 2002;20:806–810.
- Gibson L, Ashby M. *Cellular Solids: Structure and Properties*. Oxford: Pergamon; 1988.
- Elmer JW, Wong J, Ressler T. Spatially resolved X-ray diffraction phase mapping and $\alpha \rightarrow \beta \rightarrow \alpha$ transformation kinetics in the heat-affected zone of commercially pure titanium arc welds. *Metall Mater Trans A* 1998;29:2761–2773.
- Dunand DC, Bedell CM. Transformation-mismatch superplasticity in reinforced and unreinforced titanium. *Acta Mater* 1996;44:1063–1076.
- Dunand DC, Myojin S. Biaxial deformation of Ti-6Al-4V and Ti-6Al-4V/TiC composites by transformation-mismatch superplasticity. *Mater Sci Eng A* 1997;230:25–32.
- Frost H, Ashby M. *Deformation-Mechanism Maps: The Plasticity and Creep of Metals and Ceramics*. London, UK: Pergamon; 1982.
- Boyer H. *Atlas of Stress-Strain Curves*. Materials Park, OH: ASM International; 2002.
- Reed K, Brown T. Elastic, yield and ultimate properties of Emu cortical bone. *Iowa Orthop J* 2001;21:53–58.
- Shen H, Brinson L. Finite element modeling of porous titanium. *Int J Solids Struct* 2007;44:320–335.
- Thelen S, Barthelat F, Brinson L. Mechanical considerations for microporous titanium as an orthopedic implant material. *J Biomed Mater Res* 2004;69A:601–610.
- Shen H, Brinson LC. A numerical investigation of the effect of boundary conditions and representative volume element size for porous titanium. *J Mech Mater Struct* 2007;1:1179–1205.
- Li H, Oppenheimer S, Stupp S, Dunand D, Brinson L. Effects of pore morphology and bone ingrowth on mechanical properties of microporous titanium as an orthopedic implant material. *Mater Trans* 2004;45:1124–1131.

35. Pavlin D, Dove SB, Zadro R, Gluhak-Heinrich J. Mechanical loading stimulates differentiation of periodontal osteoblasts in a mouse osteoinduction model: Effect on type I collagen and alkaline phosphatase genes. *Calcif Tissue Int* 2000;67:163–172.
36. Weyts FAA, Bosmans B, Niesing R, van Leeuwen J, Weinans H. Mechanical control of human osteoblast apoptosis and proliferation in relation to differentiation. *Calcif Tissue Int* 2003;72:505–512.
37. Wolf S, Augat P, Eckert-Hubner K, Laule A, Krischak GD, Claes LE. Effects of high-frequency, low-magnitude mechanical stimulus on bone healing. *Clin Orthop Relat Res* 2001;192–198.
38. Perizzolo D, Lacefield W, Brunette D. Interaction between topography and coating in the formation of bone nodules in culture for hydroxyapatite- and titanium-coated micromachined surfaces. *J Biomed Mater Res* 2001;56:494–503.
39. Matsuzaka K, Walboomers X, Yoshinari M, Inoue T, Jansen T. The attachment and growth of osteoblast-like cells on microtextured surfaces. *Biomaterials* 2003;24:2711–2719.